
DEBLURRING IN THE WILD: A REAL-WORLD DATASET FROM SMARTPHONE HIGH-SPEED VIDEOS

A PREPRINT

Mahdi Mosh Hossain Noki

University of Dhaka

mahdimohdhossain-2019017785@cs.du.ac.bd

Syed Mumtahin Mahmud

University of Dhaka

syedmumtahin-2019617833@cs.du.ac.bd

Prothito Shovon Majumder

University of Dhaka

prothitoshovon-2018725302@cs.du.ac.bd

Abdul Mohaimen Al Radi

University of Dhaka

abdulmohaimenal-2018925300@cs.du.ac.bd

Sudipto Das Sukanto

University of Dhaka

sudiptodas-2020215639@cs.du.ac.bd

Afia Lubaina

University of Dhaka

afia-2020815624@cs.du.ac.bd

Md. Mosaddek Khan

University of Dhaka

mosaddek@du.ac.bd

August 15, 2025

ABSTRACT

We introduce the largest real-world image deblurring dataset constructed from smartphone slow-motion videos. Using 240 frames captured over one second, we simulate realistic long-exposure blur by averaging frames to produce blurry images, while using the temporally centered frame as the sharp reference. Our dataset contains over 42,000 high-resolution blur-sharp image pairs, making it approximately 10 times larger than widely used datasets, with 8 times the amount of different scenes, including indoor and outdoor environments, with varying object and camera motions. We benchmark multiple state-of-the-art (SOTA) deblurring models on our dataset and observe significant performance degradation, highlighting the complexity and diversity of our benchmark. Our dataset serves as a challenging new benchmark to facilitate robust and generalizable deblurring models. We release the dataset and generation scripts at [huggingface](https://huggingface.co).

1 Introduction

Image restoration is a widely studied field in computer vision, with research focusing on restoring image quality by removing various forms of noise including blur, haze, noise, and moiré. Image deblurring refers to the process of restoring the latent sharp image from a blurred image. Motion blur is the most common form of blur in images, and its source is diverse. Fast-moving subjects and/or camera shake can result in motion blur, as well as occlusion in motion boundaries and variation of scene depth.

Initial approaches to image deblurring [1, 2, 3, 4, 5, 6, 7, 8, 9, 10] proposed simplified mathematical models and relied on the assumption that the blur is uniform (not varying spatially across the image) or locally linear. These approaches were formulated using the following blur model:

$$B = I \otimes k + \eta$$

where I , B and k denote the sharp image, the blurred image and the blur kernel respectively. \otimes represents the convolution operation, and η denotes additive noise. The restrictive blur model and assumptions of blur uniformity across image pixels make the estimation of both I and k from B an ill-posed problem, especially when the domain consists of real-life images from various domains.

Later, machine learning based approaches have been developed for the single image deblurring problem. Earlier methods were based on convolutional neural networks (CNNs). They either involved synthesized blur images with a uniform blur kernel for training [11, 12, 13], or were trained to estimate locally linear blur kernels [14]. This is due to the absence of datasets containing real blurry images and corresponding ground truth sharp images as pairs for supervised training. More recent approaches incorporate transformers or state space models. These data-intensive approaches also often struggle to deblur images taken from real-world scenarios and suffer from a loss of generality across blurred images from all domains. For example, some methods based on generative adversarial networks (GANs) only perform well on images containing text or human faces.

The task of building a real-world dataset consisting of blurred and sharp image pairs contains multiple challenges. The primary one is ensuring the geometric and photometric alignment of the blurred image with its corresponding sharp image. The two images have to be taken at the same camera position, which is difficult because camera motion is often essential for introducing blur. There are other necessary criteria for the dataset to be realistic, such as the representation of the most common scenarios for motion blur in the dataset. The presence of noise must also be kept at a minimum level in the ground truth image.

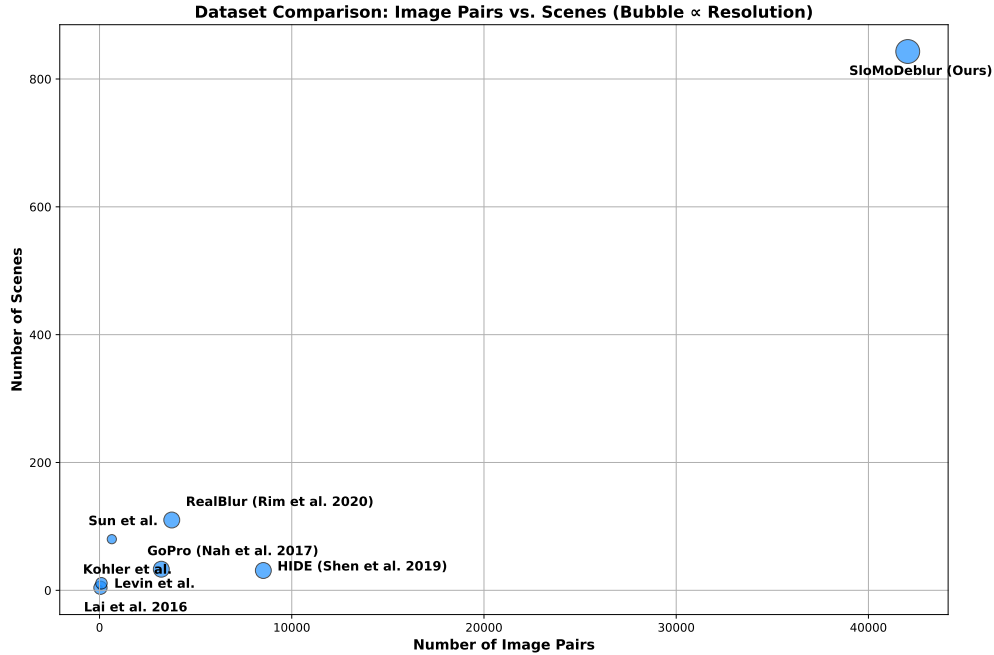


Figure 1: Comparison of SloMoDeblur dataset with other popular datasets.

Using iPhone’s 240 fps slow-motion feature, we construct long-exposure blur by averaging frames over a duration (typically 1 second) and use the middle frame as the sharp reference. This mimics physical long-exposure photography while keeping a ground-truth reference. Our dataset comprises 50,000 blur-sharp pairs, significantly larger than existing datasets such as GoPro [15] and RealBlur [16], which contain only a few thousand samples.

2 Related Works

In this section, we discuss the current models at the frontier of image deblurring and previous image deblurring datasets developed for both inference and learning.

2.1 Image Deblurring Models

The image deblurring problem is addressed in two distinct ways. The first is blind image deblurring, where the goal is to estimate the blur kernel that caused the degradation directly. Classical methods in this domain rely on strong priors or optimization techniques to infer both latent and sharp images, under the assumption of uniform or spatially-varying blur [1, 2, 3, 4, 7, 10, 12, 9, 8, 6, 5]. The second approach involves various deep learning techniques to learn a direct mapping from a blurry image to a sharp one. Deep learning based image deblurring has seen significant advancements in recent

years, with the state-of-the-art methods now achieving PSNR scores above 34 dB and SSIM values close to or exceeding 0.97. Leading approaches [17, 18] push the limits of image deblurring by leveraging adaptive reversible decoders and efficient state-space modeling, respectively. A key trend is the growing use of transformer-based architectures [19, 20, 21], which capture long-range dependencies more effectively than traditional CNNs [22, 23, 24]. Another promising direction is the integration of frequency-domain processing, as seen in models like DeepRFT+ [25] and FSNet [26], which exploit the frequency characteristics of blur. Additionally, test-time refinement techniques and lightweight models are actively researched to improve generalization and efficiency in real-world scenarios. Despite these advancements, it is challenging to handle non-uniform blur in real-world dynamic scenes and to generalize across diverse datasets. Emerging works increasingly explore self-supervised learning, Mamba-based state space models, and cross-task unification, pointing to a future where image deblurring becomes more robust and context-aware.

Several datasets have been proposed to support both learning and inference in image deblurring, and they can be broadly categorized into synthetic and real-world types. Synthetic datasets often generate blur using predefined kernels or by blending high-speed video frames, while real-world datasets aim to capture natural blur through long-exposure photography or dual-exposure setups. Many earlier datasets were primarily designed for benchmarking and kernel estimation, rather than for training deep learning models.

2.2 Synthetic Datasets

Some of the earliest synthetic deblurring datasets were designed primarily for inference and evaluation, rather than learning, due to their limited size. Levin et al. [27] introduced a dataset consisting of 32 images blurred using real camera shakes, while Sun et al. [28] proposed a synthetic dataset by convolving 80 sharp images with eight predefined blur kernels. Köhler et al. [29] further extended this idea with 48 images blurred using recorded camera motion paths to simulate spatially varying blur. While valuable for benchmarking kernel estimation methods, these datasets are too small to train deep learning models effectively. In contrast, the GoPro dataset is a large-scale synthetic dataset specifically designed for learning-based deblurring [15]. It was generated by capturing high-frame-rate video and averaging consecutive frames to simulate realistic motion blur. A similar approach was later adopted for human-centric deblurring in the HIDE dataset [30], which also uses a high-speed GoPro camera to produce synthetic blurry images of people in motion, enabling the training of models tailored to human-focused scenarios.

2.3 Real-world Datasets

Unlike synthetic datasets, real-world deblurring datasets aim to capture naturally occurring blur under authentic imaging conditions, making them more suitable for evaluating real-scene performance. Levin et al. and Kohler et al. attempted this to some extent using controlled camera motion, but these setups were still constrained and lacked scalability. Lai et al. [31] introduced a dataset of 100 real blurry images for benchmarking, but it lacked paired ground truth sharp images, limiting its utility for supervised learning. More recently, Rim et al. [16] addressed these limitations with the RealBlur dataset, which uses a hybrid camera setup to capture both long-exposure (blurred) and short-exposure (sharp) images of the same scene under natural lighting using a beam splitter. This approach produces high-quality, spatially varying real blur paired with accurate ground truth, making RealBlur one of the first real-world datasets suitable for training and evaluating deep deblurring models.

2.4 Challenges and Contributions

Despite the progress enabled by synthetic and real-world datasets, current resources remain limited in several critical aspects. Large-scale synthetic datasets like GoPro and HIDE have driven recent advances in deep learning-based deblurring, but their size and domain coverage are still constrained. GoPro contains 3,214 image pairs, while HIDE is similarly sized and focused solely on human subjects. Both are insufficient for training large modern architectures and do not generalize well to more diverse real-world scenarios.

RealBlur, one of the few real-world datasets designed for learning, improves upon earlier efforts by providing high-quality blurry-sharp pairs with better accuracy. However, it is limited in scale as well, offering fewer than 3,758 image pairs, and its data collection method introduces additional challenges. The beam splitter setup reduces the light reaching each sensor, necessitating extensive post-processing. Moreover, since the dataset was captured using DSLR cameras, the images tend to be of exceptionally high quality, failing to represent the imaging characteristics of consumer smartphones. These smartphones, with their smaller sensors and limited optics, produce more severe and complex blur due to reduced dynamic range and detail capture, conditions under which most real-world users take photos.

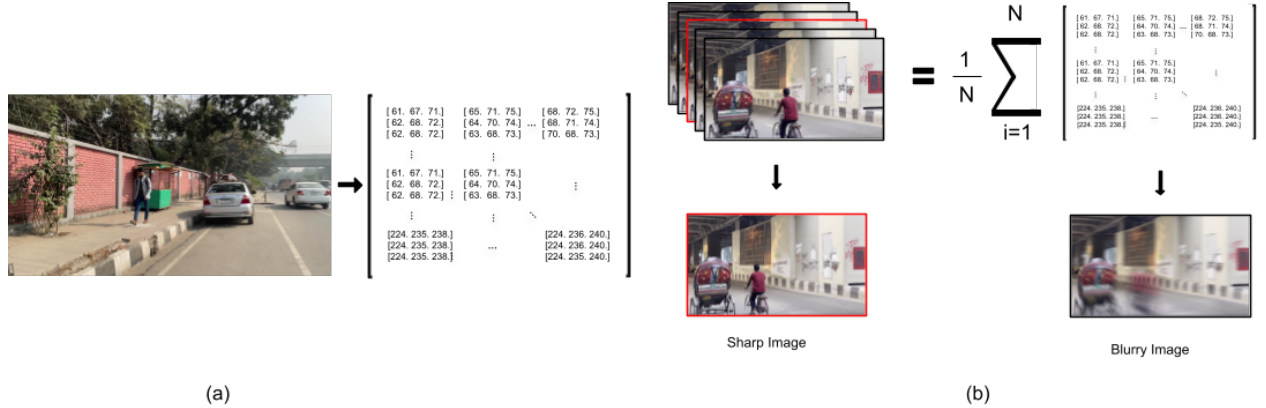
To address these limitations, we introduce a new large-scale dataset comprising over 42,000 blurry-sharp image pairs, more than ten times the size of the GoPro dataset, entirely using a modern iPhone. Using an averaging-based approach

on high-frame-rate video, we simulate realistic motion blur in unconstrained settings, while the corresponding sharp frames serve as reliable ground truth. This scale, combined with the domain relevance of smartphone imagery, positions our dataset as a new benchmark for image deblurring. It reflects the true challenges of blur encountered in everyday photography and provides a robust foundation for developing models that generalize to the most common real-world use case: photos captured by the average user on a smartphone.

3 Dataset Construction

To construct a high-fidelity dataset for training and evaluating data-driven motion deblurring algorithms, we designed a data acquisition pipeline that captures sharp and blurred image pairs under real-world conditions at the same time. We utilize the high-speed video recording capability of the iPhone 15 Pro, a modern consumer-grade smartphone equipped with an advanced imaging sensor, wide dynamic range, and computational photography pipeline. This choice of hardware serves two critical purposes: (1) it enables dense temporal sampling of real-world motion at high spatial resolution, and (2) it ensures that the resulting dataset is well-aligned with typical consumer photography scenarios, thereby improving its generalizability and real-world relevance.

We captured video sequences at a frame rate of 240 frames per second (fps) in slow-motion mode, with each frame recorded at a resolution of 1920×1080 pixels. This configuration provides both the temporal granularity needed to model motion blur formation accurately and the spatial detail necessary for fine-grained analysis of restoration performance. Additionally, utilizing a widely available mobile device rather than a specialized camera system facilitates reproducibility and lowers the barrier for future dataset expansion or adaptation.



3.1 Blur Formation Model

Motion blur occurs when the camera sensor integrates radiance from a dynamic scene over a non-zero exposure interval. Mathematically, the blur image B is modeled as:

$$B = \frac{1}{T} \int_0^T F(t) dt, \quad (1)$$

where $F(t)$ is the sharp image at time t and T is the exposure time. Since continuous integration is not feasible in digital settings, we discretize the blur as:

$$B' = \frac{1}{N} \sum_{i=0}^{N-1} F_i, \quad (2)$$

where F_i is the i -th sharp frame sampled from high-fps video. We fixed $N = 30$, resulting in an effective simulated exposure time of $T = \frac{30}{240} = \frac{1}{8}$ seconds. This simulates the blur expected in common handheld scenarios.

Algorithm 1: Create Composite Images from Video

Input: Video V with frames $V[0 \dots N - 1]$
Output: Blurred and ground truth image pairs saved to disk

```

1  $FRAMES\_TO\_LAYER \leftarrow 30;$ 
2  $frame\_itr \leftarrow 0;$ 
3 while  $frame\_itr + FRAMES\_TO\_LAYER \leq N$  do
4    $accumulator \leftarrow 0$  (empty frame);
5   for  $i \leftarrow 0$  to  $FRAMES\_TO\_LAYER - 1$  do
6      $frame \leftarrow \text{float}(V[frame\_itr + i]);$ 
7      $accumulator \leftarrow accumulator + frame;$ 
8     if  $i = \lfloor FRAMES\_TO\_LAYER/2 \rfloor$  then
9        $ground\_truth \leftarrow V[frame\_itr + i];$ 
10     $blurred \leftarrow \text{uint8}(accumulator/FRAMES\_TO\_LAYER);$ 
11    Save  $blurred$  to  $\text{images}/blurred$ ;
12    Save  $ground\_truth$  to  $\text{images}/groundtruth$ ;
13     $frame\_itr \leftarrow frame\_itr + FRAMES\_TO\_LAYER;$ 

```

The image pair generation process is detailed in Algorithm 1, which creates aligned blurred and sharp images from a high-fps video sequence.

We iterate through the video frames (ref 3 in non-overlapping segments of 30 frames (line 13). In each iteration, a temporary variable `accumulator` is initialized to hold the sum of pixel values (line 5). The midpoint frame is selected as the sharp ground truth (line 8). Once all 30 frames have been accumulated, their mean is computed and converted to construct the blurred image (line 9).

3.2 Ground Truth Definition

The central frame of the accumulation window is chosen as the ground truth sharp image:

$$F_{\text{GT}} = F_{\lfloor N/2 \rfloor}. \quad (3)$$

This choice minimizes temporal misalignment and is supported by the assumption that the motion within the short exposure interval is locally smooth. We assume the objects are in uniform motion with the very small temporal window, and with 240 fps, the center frame approximates a latent sharp image with negligible distortion.

3.3 Camera Sensor Quality

High-end DSLR cameras and devices like the GoPro HERO11 Black feature larger sensors and hardware-level stabilization, making them less susceptible to motion blur. Smartphones, including the iPhone 15 Pro, have smaller sensors and rely more on computational enhancements. However, this hardware limitation results in more frequent motion blur, which is representative of real-world scenarios. Thus, training models on smartphone-generated blur ensures better generalization to typical user environments.

3.4 Dataset Diversity and Real-World Relevance

One of the distinguishing features of our dataset is its diversity in both scene content and motion dynamics. We curated a broad spectrum of sequences that include various forms of motion, such as human activities (e.g., walking, running, hand gestures), object displacements (e.g., flying papers, swinging bags), and camera-induced movements (e.g., panning, shaking, tilting). The dataset captures both global and local motion patterns, including linear, rotational, and occlusive dynamics, as well as non-uniform motion blur resulting from depth variation and parallax.

Furthermore, because our dataset is collected using a widely adopted consumer device (the iPhone 15 Pro), it inherently incorporates the imaging characteristics typical of real-world photo and video capture pipelines. These include realistic noise levels, tone-mapping behavior, and in-camera processing features such as stabilization, denoising, and limited dynamic range compression. By reflecting the operational conditions under which end users typically capture photos, our dataset represents deployment scenarios better than datasets collected using professional, calibrated setups.

All video sequences and derived image pairs maintain a spatial resolution of **1920×1080** pixels, preserving consistency across samples. The dataset consists of high-quality (blurred, sharp) image pairs directly aligned in space and time. Unlike synthetic datasets that require explicit modeling of the camera response function (CRF) or the application of gamma correction, our dataset avoids such post-processing assumptions. Instead, we extract linear RGB data directly from the iPhone’s video stream, simplifying the data generation pipeline and enhancing physical realism.

The proposed dataset provides a high-quality, diverse, and practically relevant benchmark for learning-based motion deblurring. Its foundation in real-world hardware, natural motions, and precise blur synthesis makes it well-suited for training models that generalize to actual deployment settings, including mobile and consumer photography applications.

4 Experiments and Evaluation

This chapter presents a comprehensive evaluation of state-of-the-art image deblurring models on our proposed dataset. We begin by benchmarking several leading methods using standard quantitative metrics such as PSNR and SSIM on a substantial 10% test split, which includes approximately 4,200 high-resolution image pairs. The performance results are analyzed in the context of a baseline derived from direct blurry-to-ground-truth comparisons, highlighting the inherent difficulty of deblurring images from our dataset. In addition, we provide a comparative overview of existing deblurring datasets, emphasizing how our contribution stands out in terms of scale, diversity, and realism. Finally, we include qualitative visual results that illustrate model behavior across challenging real-world blur conditions, offering deeper insights into the strengths and limitations of current approaches.

4.1 Benchmarks

We report the performance of leading deblurring models on our dataset using PSNR and SSIM. This analysis focuses on how well each model handles the realistic and diverse blur patterns present in our test split. In addition to the quantitative results, we include a comparative overview of existing deblurring datasets to highlight how our benchmark differs in scale, complexity, and practical relevance.

Table 1: Performance of SOTA deblurring models on our dataset.

Model	PSNR (dB)	SSIM
Blurry vs. GT (baseline)	32.38	0.777
Restormer [21]	31.89	0.776
MPRNet [23]	31.98	0.785
NAFNet [32]	31.55	0.715
FFTformer [19]	32.25	0.778
DMPHN [22]	31.11	0.697
MIMO-UNet++ [24]	31.35	0.704
AdaRevD [17]	31.46	0.75

The results shown in Table 1 show that models perform significantly worse than on traditional datasets, demonstrating the difficulty of our benchmark. The average PSNR and SSIM calculated from the input blurry image and the ground truth are 32.38 and 0.777, which sets the baseline performance. None of the papers crossed the baseline PSNR, but FFTFormer exceeded SSIM than the baseline.

Table 2: Comparison of popular image deblurring datasets

Dataset	Total Pairs	Train/Test	Scenes	Res.	Type
GoPro [15]	3,214	2,103 / 1,111	33	1280×720	Synth.
HIDE [30]	8,422	6,397 / 2,025	31	1280×720	Synth. (human)
RealBlur [16]	3,758	3,058 / 700	110	1280×720	Real
Levin et al. [27]	32	–	4	255×255	Real (ctrl.)
Köhler et al. [29]	48	38 / 10	4	800×800	Real (ctrl.)
Sun et al. [28]	640	–	80	640×480	Synth.
Lai et al. [31]	100 blurry	–	100	1600×1088	Real (unpaired)
Ours	42,045	37,841 / 4,204	843	1920×1080	Synth. (phone)

Table 2 situates our dataset in the context of existing deblurring benchmarks. Compared to widely used datasets like GoPro and HIDE, our dataset is significantly larger in both the number of image pairs and scene diversity. With over 42,000 pairs across 843 distinct scenes, and a resolution of 1920×1080 , our dataset enables high-fidelity modeling of motion blur. Notably, while it is synthetically generated via frame averaging from high-frame-rate video, the use of consumer-grade smartphone footage provides realistic and diverse blur patterns that reflect real-world camera motion. This combination of scale, diversity, and realism distinguishes our dataset from others, particularly the small-scale, controlled blur datasets like Levin et al. and Köhler et al., and the relatively lower resolution and limited scenes of older benchmarks. Our contribution fills a critical gap in the deblurring literature by offering a modern, challenging dataset that better represents deployment-time scenarios.

4.2 Visual Examples

To complement our quantitative evaluation, we present a selection of qualitative examples that demonstrate the diversity and complexity of our dataset. These samples offer a visual understanding of the types of motion blur captured, as well

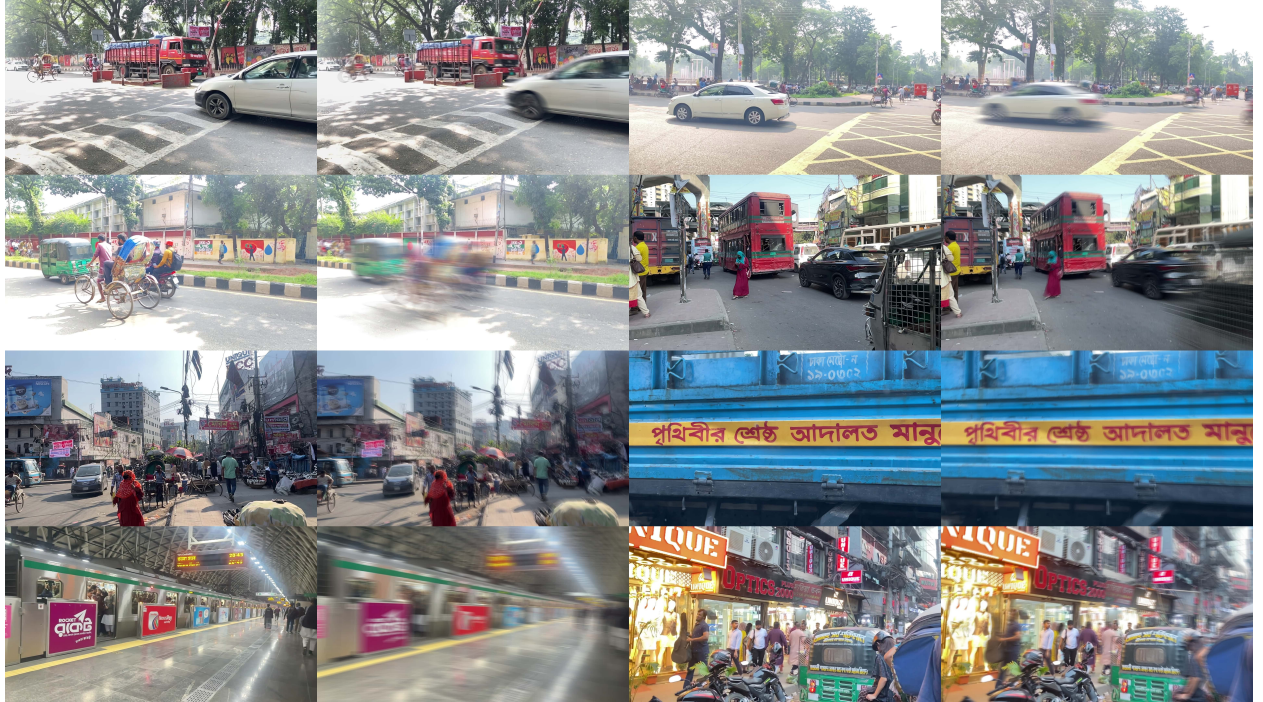


Figure 3: Paired images with sharp and blurred versions.

as the realism of the scenes. By showcasing a range of scenarios, including camera shake, fast-moving objects, and human activity, we aim to illustrate the practical challenges faced by current deblurring models.

Figure 3 showcases a diverse subset of blurry-sharp image pairs from our dataset, highlighting the variety and realism of the captured scenes. The examples include a wide range of motion types such as object motion, human activity, and camera shake. It also captures a range of lighting conditions and depths of field. These samples illustrate the presence of complex and spatially varying lighting conditions often found in real-world scenarios.

5 Conclusion

In this work, we have introduced a novel large-scale real-world image deblurring dataset constructed from high-frame-rate smartphone video, addressing critical limitations of existing benchmarks in scale, realism, and domain relevance. By leveraging the iPhone 15 Pro’s 240 fps slow-motion capture, we synthesized realistic motion blur through temporal averaging and paired each blurred image with a temporally aligned sharp ground truth. This methodology yielded over 42,000 high-resolution blur-sharp pairs encompassing diverse scenes and motion patterns, significantly surpassing the scale of prior datasets.

Our comprehensive benchmarking of state-of-the-art deblurring models, including transformer-based architectures and frequency-domain approaches, revealed substantial performance degradation when evaluated on our dataset. This underscores the dataset’s complexity and reflects the challenges it poses to existing deblurring techniques, highlighting the need for more robust and generalizable models.

5.1 Limitations

While our dataset represents a significant step forward in realistic motion deblurring benchmarks, it is not without limitations. First, all scenes were recorded under well-lit conditions, primarily during daylight or in well-lit indoor environments, which means low-light scenarios are underrepresented despite being common in real-world photography. Additionally, all benchmark results were obtained using publicly available pretrained models without fine-tuning on our dataset; while this highlights generalization gaps, it may not reflect each model’s full potential performance on our data. The dataset also lacks diversity in capture devices, as all videos were recorded using a single smartphone model. This may limit the generalizability of results to other hardware with different optical or sensor characteristics. Finally, although we report standard quantitative metrics like PSNR and SSIM, we do not include a human perceptual evaluation, which would provide complementary insights into real-world deblurring quality, particularly in complex or ambiguous cases where numerical scores may not correlate with subjective preference.

5.2 Future Work

Building on the strengths of our dataset, several directions can be pursued to enhance its scope and applicability. One natural extension is to incorporate low-light and nighttime capture conditions, which would expose models to more challenging scenarios involving noise, reduced dynamic range, and sensor non-linearities. Adding data from a broader range of devices including lower-end smartphones, tablets, and action cameras could further diversify the imaging characteristics and improve model robustness across hardware variations. Another promising avenue is to augment the dataset with precise motion metadata, such as gyroscope or optical flow data, which can enable the development of motion-aware or physics-informed deblurring models. Furthermore, collecting user ratings or conducting perceptual studies would help complement traditional metrics like PSNR and SSIM with human-centered evaluations, providing a more comprehensive understanding of visual quality. Finally, leveraging our dataset for training generative or diffusion-based models could open new paths for perceptually grounded and temporally consistent deblurring performance.

By providing a dataset that closely mirrors real-world conditions encountered in everyday smartphone photography, we offer a valuable resource for developing and evaluating advanced deblurring algorithms. We anticipate that this dataset will catalyze further research into models that can effectively handle the intricacies of real-world motion blur, ultimately advancing the field of image restoration.

References

- [1] A. Gupta, N. Joshi, C. Zitnick, M. Cohen, and B. Curless, “Single image deblurring using motion density functions,” vol. 6311, pp. 171–184, 09 2010.
- [2] O. Whyte, J. Sivic, A. Zisserman, and J. Ponce, “Non-uniform deblurring for shaken images,” vol. 98, pp. 491–498, 06 2010.
- [3] S. Harmeling, H. Michael, and B. Schölkopf, “Space-variant single-image blind deconvolution for removing camera shake,” in *Advances in Neural Information Processing Systems* (J. Lafferty, C. Williams, J. Shawe-Taylor, R. Zemel, and A. Culotta, eds.), vol. 23, Curran Associates, Inc., 2010.
- [4] M. Hirsch, C. J. Schuler, S. Harmeling, and B. Schölkopf, “Fast removal of non-uniform camera shake,” in *2011 International Conference on Computer Vision*, pp. 463–470, 2011.
- [5] S. Cho and S. Lee, “Fast motion deblurring,” *ACM Trans. Graph.*, vol. 28, 12 2009.
- [6] J. Pan, D. Sun, H. Pfister, and M.-H. Yang, “Deblurring images via dark channel prior,” *IEEE Trans. Pattern Anal. Mach. Intell.*, vol. 40, no. 10, pp. 2315–2328, 2018.
- [7] R. Fergus, B. Singh, A. Hertzmann, S. T. Roweis, and W. T. Freeman, “Removing camera shake from a single photograph,” *ACM Trans. Graph.*, vol. 25, p. 787–794, July 2006.
- [8] Q. Shan, J. Jia, and A. Agarwala, “High-quality motion deblurring from a single image,” *ACM Trans. Graph.*, vol. 27, p. 1–10, Aug. 2008.

[9] L. Xu and J. Jia, “Two-phase kernel estimation for robust motion deblurring,” in *Computer Vision – ECCV 2010* (K. Daniilidis, P. Maragos, and N. Paragios, eds.), (Berlin, Heidelberg), pp. 157–170, Springer Berlin Heidelberg, 2010.

[10] L. Xu, S. Zheng, and J. Jia, “Unnatural l0 sparse representation for natural image deblurring,” in *2013 IEEE Conference on Computer Vision and Pattern Recognition*, pp. 1107–1114, 2013.

[11] A. Chakrabarti, “A neural approach to blind motion deblurring,” 03 2016.

[12] C. J. Schuler, M. Hirsch, S. Harmeling, and B. Schölkopf, “Learning to deblur,” *IEEE Transactions on Pattern Analysis and Machine Intelligence*, vol. 38, no. 7, pp. 1439–1451, 2016.

[13] L. Xu, J. S. J. Ren, C. Liu, and J. Jia, “Deep convolutional neural network for image deconvolution,” in *Proceedings of the 28th International Conference on Neural Information Processing Systems - Volume 1*, NIPS’14, (Cambridge, MA, USA), p. 1790–1798, MIT Press, 2014.

[14] J. Sun, W. Cao, Z. Xu, and J. Ponce, “Learning a convolutional neural network for non-uniform motion blur removal,” in *2015 IEEE Conference on Computer Vision and Pattern Recognition (CVPR)*, (Los Alamitos, CA, USA), pp. 769–777, IEEE Computer Society, June 2015.

[15] S. Nah, T. H. Kim, and K. M. Lee, “Deep multi-scale convolutional neural network for dynamic scene deblurring,” in *CVPR*, July 2017.

[16] J. Rim, H. Lee, J. Won, and S. Cho, “Real-world blur dataset for learning and benchmarking deblurring algorithms,” in *Computer Vision – ECCV 2020: 16th European Conference, Glasgow, UK, August 23–28, 2020, Proceedings, Part XXV*, (Berlin, Heidelberg), p. 184–201, Springer-Verlag, 2020.

[17] X. Mao, Q. Li, and Y. Wang, “Adarevd: Adaptive patch exiting reversible decoder pushes the limit of image deblurring,” pp. 25681–25690, 06 2024.

[18] L. Kong, J. Dong, M.-H. Yang, and J. Pan, “Efficient visual state space model for image deblurring,” 2024.

[19] L. Kong, J. Dong, J. Ge, M. Li, and J. Pan, “Efficient frequency domain-based transformers for high-quality image deblurring,” in *Proceedings of the IEEE/CVF Conference on Computer Vision and Pattern Recognition (CVPR)*, pp. 5886–5895, June 2023.

[20] X. Mao, J. Wang, X. Xie, Q. Li, and Y. Wang, “Loformer: Local frequency transformer for image deblurring,” 07 2024.

[21] S. W. Zamir, A. Arora, S. Khan, M. Hayat, F. S. Khan, and M. Yang, “Restormer: Efficient transformer for high-resolution image restoration,” in *2022 IEEE/CVF Conference on Computer Vision and Pattern Recognition (CVPR)*, pp. 5718–5729, 2022.

[22] H. Zhang, Y. Dai, H. Li, and P. Koniusz, “Deep stacked hierarchical multi-patch network for image deblurring,” in *The IEEE Conference on Computer Vision and Pattern Recognition (CVPR)*, June 2019.

[23] S. W. Zamir, A. Arora, S. Khan, M. Hayat, F. S. Khan, M.-H. Yang, and L. Shao, “Multi-Stage Progressive Image Restoration,” in *2021 IEEE/CVF Conference on Computer Vision and Pattern Recognition (CVPR)*, (Los Alamitos, CA, USA), pp. 14816–14826, IEEE Computer Society, June 2021.

[24] S.-J. Cho, S.-W. Ji, J.-P. Hong, S.-W. Jung, and S.-J. Ko, “Rethinking coarse-to-fine approach in single image deblurring,” in *2021 IEEE/CVF International Conference on Computer Vision (ICCV)*, pp. 4621–4630, 2021.

[25] X. Mao, Y. Liu, F. Liu, Q. Li, W. Shen, and Y. Wang, “Intriguing findings of frequency selection for image deblurring,” *Proceedings of the AAAI Conference on Artificial Intelligence*, vol. 37, pp. 1905–1913, Jun. 2023.

[26] Y. Cui, W. Ren, X. Cao, and A. Knoll, “Image restoration via frequency selection,” *IEEE Transactions on Pattern Analysis and Machine Intelligence*, 2023.

[27] A. Levin, Y. Weiss, F. Durand, and W. T. Freeman, “Understanding and evaluating blind deconvolution algorithms,” in *2009 IEEE Conference on Computer Vision and Pattern Recognition*, pp. 1964–1971, 2009.

[28] L. Sun, S. Cho, J. Wang, and J. Hays, “Edge-based blur kernel estimation using patch priors,” in *IEEE International Conference on Computational Photography (ICCP)*, pp. 1–8, 2013.

[29] R. Köhler, M. Hirsch, B. J. Mohler, B. Scholkopf, and S. Harmeling, “Recording and playback of camera shake: Benchmarking blind deconvolution with a real-world database,” in *European Conference on Computer Vision*, 2012.

[30] Z. Shen, W. Wang, J. Shen, H. Ling, T. Xu, and L. Shao, “Human-aware motion deblurring,” in *IEEE International Conference on Computer Vision*, 2019.

- [31] W.-S. Lai, J.-B. Huang, Z. Hu, N. Ahuja, and M.-H. Yang, “A Comparative Study for Single Image Blind Deblurring,” in *2016 IEEE Conference on Computer Vision and Pattern Recognition (CVPR)*, (Los Alamitos, CA, USA), pp. 1701–1709, IEEE Computer Society, June 2016.
- [32] L. Chen, X. Chu, X. Zhang, and J. Sun, “Simple baselines for image restoration,” *arXiv preprint arXiv:2204.04676*, 2022.